

**ICSV14**  
Cairns • Australia  
9-12 July, 2007



## **SPECTRAL CHARACTERISTICS OF WALL PRESSURE FLUCTUATIONS FOR SURFACE SHIPS**

Riccardo Broglio<sup>1</sup>, Elena Ciappi<sup>1</sup>, Andrea Di Mascio<sup>1</sup>, Francesca Magionesi<sup>1</sup>

<sup>1</sup>INSEAN-Istituto Nazionale per Studi ed Esperienze di Architettura Navale  
Via di vallerano 139, 00128 Rome, Italy  
[a.dimascio@insean.it](mailto:a.dimascio@insean.it)

### **Abstract**

Wall pressure fluctuations generated by the turbulent boundary layer (TBL) which extends on the wall of moving vehicles, play an important role in the mechanism of noise generation through fluid-structure coupling. In the case of marine applications, the calculation and the suppression of the radiated noise is crucial to ensure sonar efficiency as well as to improve the comfort level on board new high speed vessels for passenger transportation.

The studies performed in this field, most of them devoted to aeronautical applications and based on the analysis of experimental data, deal with equilibrium flow for which scaling laws for the power spectral density and theoretical models for the cross spectral density are available.

The problem in the case of marine vehicles presents some peculiarities because of pressure gradients due to both free surface and hull curvature.

Their effects on wall pressure spectra are in this work analyzed comparing pressure experimental data measured in different locations along the hull where favorable, adverse and zero pressure gradients are present. These particular zone are identified by analyzing the mean velocity and pressure field obtained by RANS numerical simulations. The results of this analysis provides interesting information on the characteristics of wall pressure spectra and on the validity of the scaling laws for the power spectral density in the presence of pressure gradients.

### **1. INTRODUCTION**

Vibrations of elastic structures excited by the turbulent boundary layer are of interest for interior and exterior noise emission problems in aeronautical, automotive and, due to the considerable increase of the velocity of passenger ships, in marine applications.

The typical way to characterise wall pressure fluctuations (WPF) is via experimental tests performed in suitable facilities, mainly wind or water tunnels. In fact, direct numerical simulations (DNS) or large eddy simulations (LES) are often not applicable in the case of complex geometries and realistic flow conditions (high Reynolds number flows) due to the limitation of computational resources. Direct numerical simulations of WPF were performed by Choi and Moin [1] analysing the channel flow problem for  $Re_g = 287$ . Recently, Lee et al. [2] proposed a new methodology to calculate numerically wall pressure spectra. The method

uses the predicted mean flow field obtained from RANS calculations and a spectral correlation model, and integrates across the turbulent boundary layer. The method was validated for both an equilibrium flow for  $Re_g = 3582$  and a nonequilibrium flow over a backward-facing step. Equilibrium pressure gradient effects on wall pressure spectra were analysed theoretically and numerically by Panton and Linebarger[3].

On the other side, there are many experimental works related to WPF, most of them related to the identification of the appropriate scaling laws for the power spectral density (PSD) for zero pressure gradient flow [4]. The pressure PSD frequency range is subdivided according to the boundary layer regions that give contributions to wall pressure spectra where different scaling variables hold. In particular, Farabee and Casarella [5] identified four frequency ranges in their data: the low frequency and the mid-frequency range where outer variables hold, the high frequency range where inner variables hold, and an overlap scale-independent region proportional to  $\omega^{-1}$ , being  $\omega$  the circular frequency, whose extent depends on the Reynolds number. In [6] another confirmation of the validity of the scaling laws suggested by Farabee and Casarella is provided.

In the present work a RANS code is utilized to characterize the mean velocity and pressure field around an high speed catamaran. The obtained results allowed the identification of particular hull sections where pressure gradient effects can be important. The analysis of pressure signals shown that the classical outer scaling laws do not provide a clustering of the pressure spectra when both favorable or adverse pressure gradients are present. In particular pressure gradient effects result in a higher level of the scaled pressure spectra at low frequency with respect to the zero pressure gradient case. It is also addressed that an adverse pressure gradient of the same entity of a favorable one produces more significant effects on pressure spectra.

## 2 NUMERICAL ANALYSIS OF THE VELOCITY FIELD AROUND

### 2.1 Flow solver

The code used for the simulation of the flow past the catamaran is a general purpose, finite volume, second-order solver, based on an integral formulation of the Navier-Stokes equations [7]. In particular, the convective and pressure terms are solved by means of a second order ENO formulation [8], whereas the viscous terms are approximated by a second order centered scheme. The code can handle several turbulence models for the closure of the Reynolds stresses (algebraic, one-equation or two equation). In the results reported in the following, the turbulent viscosity has been calculated by means of the Spalart-Allmaras model [9]. For the simulation of free surface effects, a single-phase level set algorithm is adopted, i.e. only the liquid phase of the fluid is computed [7]. When computing unsteady flows, the time derivatives are approximated by means of a second order accurate three-points backward finite difference approximation formula.

Pressure-velocity coupling and the solution of the solenoidal constrain (divergence-free flow) are obtained by the pseudo-compressibility formulation and the introduction of a dual (or pseudo) time-derivative in the discrete system of equations. The solution at each time step is then obtained as the steady state with respect to the pseudo-time parameter. The integration with respect to the pseudo time is carried out by an implicit Euler scheme with approximate factorization, and a local dual time step and a multi-grid technique have been used to improve the convergence rate of the sub-iteration. Finally, the code has been parallelized by both MPI procedures and OMP directives, in order to exploit both distributed and shared memory parallel algorithms on clusters of multiprocessor nodes.

## 2.2 Numerical results

The numerical simulations were performed on a 1:15 model of the fast catamaran Jumbo CAT (see figure 1). The scale of the model, chosen to fulfill experimental facilities constraints, is based on the Froude similarity:  $Fr = U / \sqrt{gL_{pp}}$  where  $U$  is the ship speed,  $g$  is the acceleration of gravity and  $L_{pp}$  is the length between perpendicular. Therefore, the maximum model width is 1.467m,  $L_{pp}$  is 4.38m and its draft  $d$ , in calm water conditions, is 0.2 m.

The flow past the catamaran has been simulated for several speed conditions, ranging from 25 to 40 knots, corresponding to  $Fr=0.49$  and  $Fr=0.78$ , respectively.

In what follows  $x$  denotes the longitudinal axis ( $x=0$  and  $x=1$  corresponds to the forward and to the aft perpendicular, respectively),  $y$  the transversal axis and  $z$  the vertical axis (positive upward, with  $z=0$  on the keel line).



Figure 1 Catamaran model and test sections for pressure measurements

A multi-block grid with 28 structured blocks and a total of about  $6 \times 10^5$  grid points and 5 grid levels for multi-grid acceleration has been used for all the simulations. The computed free surface for 25 and 40 knots are reported in Figure 2.

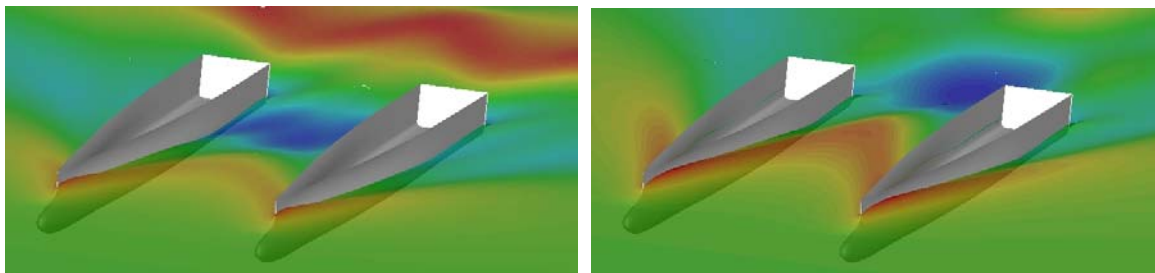


Figure 2: Free surface contours; Left: 25 Kn, Right: 40 Kn

As it can be clearly seen from the picture, as the speed increases, the trough between the demihulls shift backward; consequently, the pressure minimum on the hull surface and the related pressure gradients move backward as well, as it can be seen in Figure.3. It can also be noticed that pressure gradients are more intense for the lower speed condition (25 Kn).

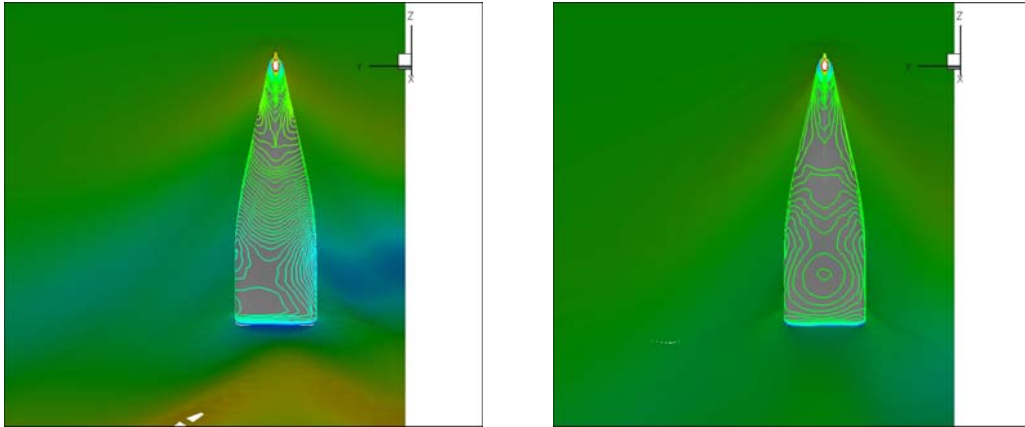


Figure 3: Pressure contours on the hull  $-0.1 < p < 0.1$   $\Delta p = 0.001$ ; Left: 25 Kn, Right: 40 Kn

As consequence of the shift in pressure gradients and pressure extrema, a remarkable distortion of the boundary layer on the hull (and of the wake behind, with a large widening of the wake for the lower speed, caused by the local maximum in the wave height downstream the stern, as seen in figure 2) can be observed in Figure 4, where the velocity contours are plotted on several cross sections.

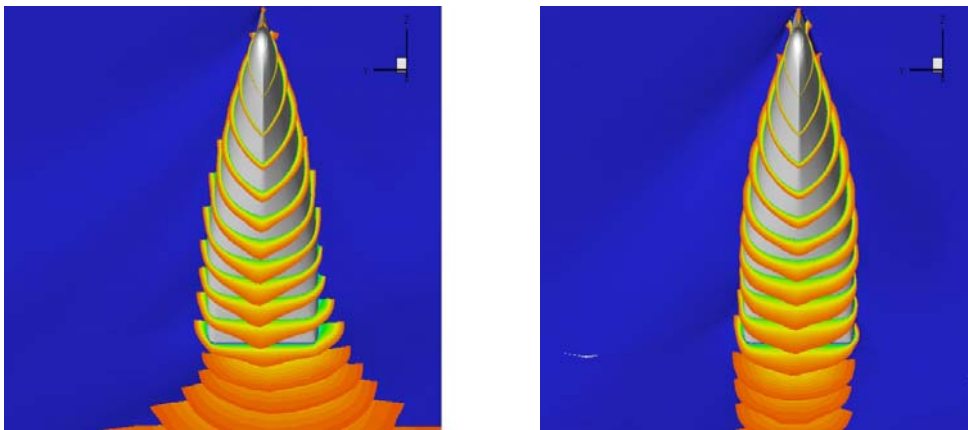


Figure 4: Velocity contours along the hull  $0 < u < 0.95$   $\Delta u = 0.05$ ; Left: 25 Kn, Right: 40 Kn

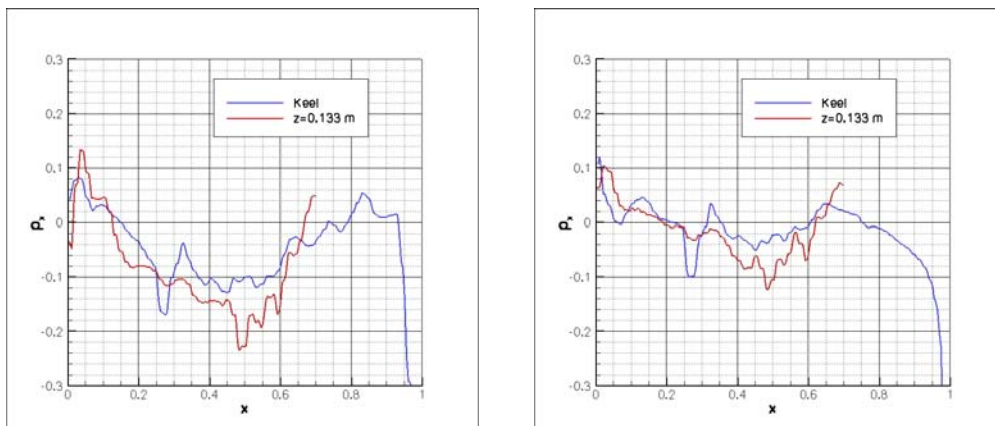


Figure 5: Pressure gradients. Left: 25 Kn, Right: 40 Kn

Finally, in Figure 5 pressure gradients values are shown in correspondence to the keel line and to a longitudinal section at  $z=0.113$  where the hull curvature presents a maximum. From the inspection of these figures it is evident that the higher pressure gradients are found

in both cases at the bow ( $0.03 < x < 0.1$ ) and in the middle of the model ( $x \sim 0.5$ ); however they are much more pronounced for the lowest velocity case. Moreover, pressure gradients reach a local minimum at the keel line in correspondence of the stern part of the hull.

### 3 EXPERIMENTAL ANALYSIS OF WALL PRESSURE SPECTRA

#### 3.1 Experimental set-up

The experiments performed on the 1:15 model of the fast catamaran Jumbo CAT were carried on in the INSEAN towing tank n. 2 (see Figure 1) that is 220 m long, 9 m wide and 3.5m deep and it is equipped with a carriage that can reach a maximum speed of 8 m/s. The use of this kind of facility creates ideal flow conditions because background turbulence and noise are avoided. Three sections were chosen to perform pressure measurements. On the basis of the results shown in Figures 5, the first test section was located in the bow part of the model at  $x=0.05L_{pp}$  and  $z=0.113$  m where an adverse pressure gradient is present, the second section at  $x=0.5L_{pp}$  and  $z=0.113$  m where a favorable pressure gradient is present instead. The third section was chosen in the stern part of the ship bottom  $x=0.86L_{pp}$  where pressure gradient values are close to zero. The basic setup consisted in an array of 9 transducers in streamwise direction and, only in the stern section, of 5 transducers in crosswise direction mounted flush with the plate at constant distance between each other of 1 cm. Additional tests were performed in the stern section with 13 transducers mounted in streamwise direction within a maximum distance of 40 cm. These additional measurements as well as those performed in crosswise direction were devoted to cross spectral density analyses (for the details see [10]). The turbulent boundary layer local characteristics in correspondence of the test sections are reported in Table 1. Pressure signals were acquired in calm water conditions with fixed trim and sinkage and for four different ship model velocities ranging from 3.31 m/s to 5.3 m/s, corresponding to 25 and 40 knots, respectively.

Mean flow parameters: bow section				
Speed (knots)	Speed (m/s)	$\delta$ (m)	$\delta^*$ (m)	$u_\tau$ (m/s)
25	3.31	$1.38 \cdot 10^{-2}$	$1.726 \cdot 10^{-3}$	0.126
40	5.3	$1.23 \cdot 10^{-2}$	$1.53 \cdot 10^{-3}$	0.199
Mean flow parameters: mid section				
25	3.31	$2.32 \cdot 10^{-2}$	$2.89 \cdot 10^{-3}$	0.127
40	5.3	$4.08 \cdot 10^{-2}$	$5.1 \cdot 10^{-3}$	0.179
Mean flow parameters: stern section				
25	3.31	0.12	0.0142	0.11
40	5.3	0.113	0.0137	0.1626

Table 1 Mean flow velocity parameters

Differential piezoresistive pressure transducers Endevco 8510-B, characterised by a rectangular sensing element area of  $1 \times 0.3 \text{ mm}^2$ , a maximum range of 2 psig and by a certified flat response until 14 kHz were used to measure pressure fluctuations. Pressure signals were acquired and amplified by the 16 channels acquisition system PROSIG; the

sampling frequency was 12.5 kHz, the acquisition time varies between 15 and 30 s depending on the model speed. Several repetitions of the test were performed to obtain a significant statistics.

### 3.2 Wall pressure spectra in zero pressure gradients flow

The results shown in this section refer to pressure measurements performed in the stern section where pressure gradients are supposed to be negligible. In particular only pressure data acquired for 3.31m/s (25 Knots) and 5.3m/s (40 Knots) are here presented. For these model velocities  $Re_g = U\vartheta/\nu$  varied between  $2.9 \cdot 10^4$  and  $4.28 \cdot 10^4$ ,  $\vartheta$  being the momentum thickness and  $\nu$  the cinematic viscosity. Experimental data were processed to derive the power spectral densities (PSD)  $\Phi_{pp}(\omega)$ . In Figure 6 the PSD for the two different test velocities, scaled with outer variables:  $\omega\delta/u_\tau$ ,  $\phi_{pp}u_\tau/\tau_w^2\delta$  where  $\delta$  is the TBL thickness,  $u_\tau$  is the friction velocity and  $\tau_w = u_\tau^2\rho$  is the shear stress, are shown and compared with the results of Farabee and Casarella [5] obtained for  $Re_g = 6050$  and with the results of Blake [3] obtained for  $Re_g = 8210$ . It is evident an excellent collapse of the present data for the mid frequencies *i.e.* for  $20 < \omega\delta/u_\tau < 2000$  and, for  $\omega\delta/u_\tau < 800$ , a very good agreement with the Farabee and Casarella curve and in fair agreement with Blake data. Moreover the scaled spectra achieved the maximum value for  $\omega\delta/u_\tau \approx 55$ .

Figure 7 shows the present wall pressure spectra and the results of Bull and Thomas [4], Farabee and Casarella and Blake scaled on inner flow variables:  $\omega\nu/u_\tau^2$ ,  $\phi(\omega)u_\tau^2/\tau_w^2\nu$ . According to Blake [11], attenuation in the spectra should occur approximately for  $\omega d/U > 1.2$  that implies  $\omega\nu/u_\tau^2 > 0.3$  or  $0.42$  depending on flow velocity. A collapse of the two set of measurements occurs for  $0.045 < \omega\nu/u_\tau^2 < 0.32$ . Bull and Thomas' and Blake's data are in excellent agreement in the same frequency range. On the contrary, Farabee and Casarella curve show a quite different trend characterised by a slower high frequency decay. Differences can be due to spectra attenuation caused by the finite sensor dimensions and, when considering the same  $d^+ = du_\tau/\nu$  values, to the use of different pressure transducers. Finally the overlap region, due to the quite high Reynolds values, had a considerable extension. The  $\omega^{-1}$  law is included in both figures 6 and 7, showing that the overlap region extends in the range  $0.03 \approx 300/R_\tau < \omega\nu/u_\tau^2 < 0.174$ . The current results agree very well with those provided in [6] obtained in a different facility, for a different ship model and for  $Re_g$  values ranging between 4530 and 14200.

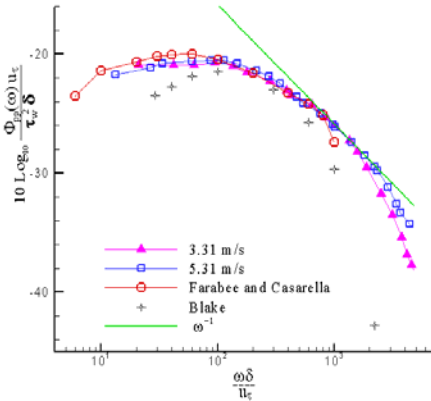


Figure 6: PSD scaled with outer variables

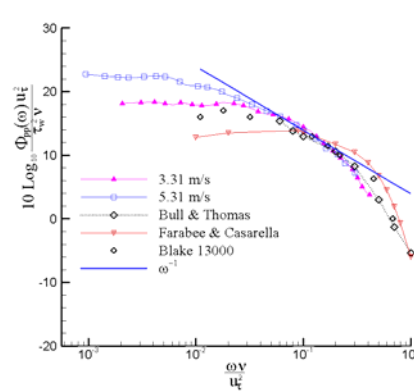


Figure 7: PSD scaled with inner variables

### 3.3 Wall pressure spectra in presence of pressure gradients

In this section comparisons between pressure spectra measured in an adverse, in a favourable and in an almost zero pressure gradient flow is presented. In Figure 8 the PSD scaled on outer flow variables are shown for the lowest velocity case. It is evident that outer scales do not provide a collapse of the three curves. However, both the adverse and the favorable pressure gradient produce an higher level in the low frequency part of the spectra with respect to the zero pressure gradient case. Moreover, although the favourable pressure gradient has a value that is twice that of the adverse pressure gradient (see Figure 5) the corresponding pressure spectra show a quite similar trend. Analogous conclusions can be drawn for the highest velocity case as clearly shown in Figure 9. In this case, although the two pressure gradient values are of the same order (see Figure 5), the spectrum measured in presence of the favourable one is significantly lower than that measured in presence of the adverse pressure gradient. From the above considerations it can be concluded that the effects produced by an adverse pressure gradient on wall pressure spectra are more pronounced than that produced by a favourable pressure gradient of the same entity. Panton and Linebarger [3] analysing the effect of different adverse equilibrium pressure gradient flows on pressure spectra found the same low frequency behaviour except for the fact that in correspondence of the overlap region all the curves collapsed indicating that pressure gradients had no effects in this region. Unfortunately, in the present case, the universal scale-independent region is not visible for the bow and for the mid hull pressure spectra because of the low values of the local Reynolds numbers.

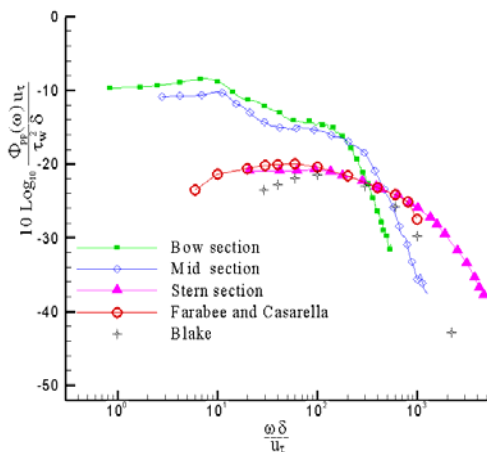


Figure 8: PSD scaled with outer variables.  
U=25 Knots

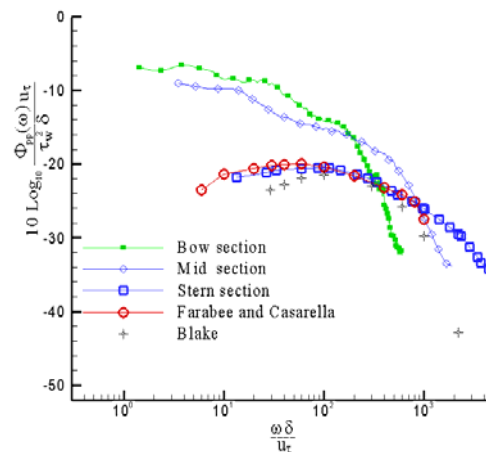


Figure 9: PSD scaled with outer variables .  
U=40 Knots

## CONCLUSIONS

In this work an analysis of wall pressure measurements performed on a fast catamaran in three different sections characterised by an adverse, a favorable and a zero pressure gradient is presented. A strong dependency of the PSD on the pressure gradients when using the outer flow parameters to scale the low frequency part of the spectra suggests the need of choosing new set of parameters to take into account for this effect.

## ACKNOWLEDGEMENTS

This work has been support by the Ministero dei Trasporti in the frame of “Programma Ricerche 2007-2009”.

## REFERENCES

1. H., Choi, P., Moin, “On the Space-Time Characteristics of Wall Pressure Fluctuations”, *Physics of Fluids A* **2**, 1450-1460 (1990).
2. Y.T. Lee, W.K. Blake and T.M. Farabee, “Modeling of Wall Pressure Fluctuations Based on Time Mean Flow Field”, *Journal of Fluids Engineering* **127**, 233-240 (2005).
3. R. L., Panton, J. H., Linebarger, “ Wall pressare spectra calculations for equilibrium boundary layers”, *Journal of Fluid Mech*, **65** (2), 261-287 (1974).
4. W.L., Keith, D.A., Hurdis and B.M., Abraham, “A Comparison of Turbulent Boundary Layer Wall-Pressure Spectra”, *ASME Journal of Fluids Engineering* **114**, 338-347 (1992).
5. T. M. Farabee and M.J. Casarella, “Spectral Features of Wall Pressure Fluctuations beneath Turbulent Boundary Layers”, *Physics of Fluids A* **3**, 2410-2420, (1991).
6. E., Ciappi, F., Magionesi, “Characteristics of the Turbulent Boundary Layer Pressure Spectra for High Speed Vessels”, *Journal of Fluid and Structures* **21**(3) (2005).
7. A., Di Mascio, R., Broglia and R., Muscari, “On the Application of the Single-Phase Level Set Method for Naval Hydrodynamic Flows”, *Comp. and Fluids* **36**, 868-886 (2007).
8. A., Harten, B., Engquist, S., Osher, and S. R., Chakravarthy, “Uniformly High Order Accurate Essentially Non-Oscillatory Schemes”. *J. Comput. Phys.* **71**,231–303 (1987).
9. P.R., Spalart, S.R., Allmaras, “A One-Equation Turbulence Model for Aerodynamic Flows”, in *AIAA-92-0439, AIAA 30th Aerospace Sciences Meeting* (1992).
10. E. Ciappi and F. Magionesi, “Prediction of the Noise Level Generated by the Turbulent Boundary Layer on Board a Fast Ship”, *Internoise2006*, Honolulu, U.S (2006).
11. W.K., Blake, *Mechanics of Flow Induced Sound and Vibration*, Academic Press, Orlando (1986).